

## Analytical Solution for Single and Multiple impacts with Strain-rate Effects for Shot Peening

Baskaran Bhuvanaraghan<sup>1</sup>, Sivakumar M Srinivasan<sup>2</sup>  
Bob Maffeo<sup>3</sup> and Om Prakash<sup>4</sup>

**Abstract:** Shot peening is a complex and random process which is controlled by many input parameters. Numerical methods, which are normally used for impact problems will prohibitively put strain on the computing resources since a large number of impacts are involved in the computations. In this paper, a simplified analytical approach is used to predict the residual compressive stress that includes strain-rate effects. This is based on the method proposed by Shen and Atluri (2006) with a simple modification to include the strain rate effects. The residual stresses are predicted in materials SAE1070 and Inco718. In the computations, the random variation of the input parameters are simulated to predict the residual stress variation using the Monte-Carlo method. The stress distributions computed using the analytical method compare well with the direct numerical methods and the experimental results.

**Keywords:** Shot peening, Analytical method, Residual stress.

### 1 Introduction

Shot peening is a cold working process in which metallic components are subjected to random impacts of shots. It is employed to impart residual compressive stresses(RCS) on the metallic surfaces. Besides the fact that a large number of shots and the random nature of the process are to be modeled, the number of input parameters are also many. For example, shot size, velocity, angle, material hardness, target material hardness, friction etc. play a role in the determination of RCS (Nikulari, 1981). Therefore, it is overly exhaustive to model the process completely by using any numerical methods. The current techniques employed are based mostly

---

<sup>1</sup> GE Aviation, Bangalore, India.

<sup>2</sup> Professor, Applied Mechanics, IIT Madras, Chennai.

<sup>3</sup> Consulting Engineer, GE Aviation, USA.

<sup>4</sup> GE Global Research, Bangalore

on the Finite Element Method(FEM) and generally use a unit cell approach with a limited number of shots.

Analytical methods provide quick and approximate results. Hertzian theory based on elastic indentation is the first attempt to model a single shot impact analytically. This theory is extended to include the plastic zone formation during the impact. Johnson (1987) proposed a spherical cavity with hydrostatic pressure loading to analyze the stresses in the plastic and the adjacent elastic zones. Al-Hassani (1984) added causal or source stress to the bending and axial stresses to evaluate the residual stress in a thin plate. Al-Obaid (1995) predicted the source stress to be a cosine function. Shen and Atluri (2006) recently extended the analytical method proposed by Li and co workers (Li, Mei, Duo, and Renzhi, 1991) to predict the residual stresses. This method uses a linear hardening material model and reverse yielding for rate-independent plastic deformations.

In this paper, equations representing the single-shot impact are presented by enhancing the method proposed by Shen and Atluri (2006) to include strain-rate effects, using Johnson-Cook model. In addition, the elastic-plastic stresses and strains are calculated using Neuber's equation, instead of using the ratio of elastic and plastic indentations adopted by Shen and Atluri (2006). The residual stresses are compared with numerical results obtained from ABAQUS software. In reality, the entire surface is shot-peened leading to in-plane residual compressive stresses. The in-plane strains are only functions of depth direction. For multiple shots, averaging of plastic strains along indentation is used to calculate the residual stresses on the surface. The results are compared with the results from FEM analysis with multiple shot-impacts as well as experimental results reported in the literature. Monte-Carlo simulations are carried out to enhance the prediction capability catering to random variation of input parameters.

## **2 Analytical modeling of shot peening**

The main assumptions made in this analytical method are:

- 1) The body is semi-infinite
- 2) The material is isotropic as well as strain-rate dependent and strain-hardening
- 3) The impacts are normal to the target surface
- 4) During the impact, there is no friction, rolling, or slip
- 5) The indenter is spherical in shape

### ***2.1 Formulation for a single shot based on Shen and Atluri model***

In this formulation, first, the maximum stresses under the loading due to a single shot impact assuming the material is purely elastic are obtained. This is reproduced from the work of (Shen and Atluri, 2006) for the sake of completeness in 2.1.1.

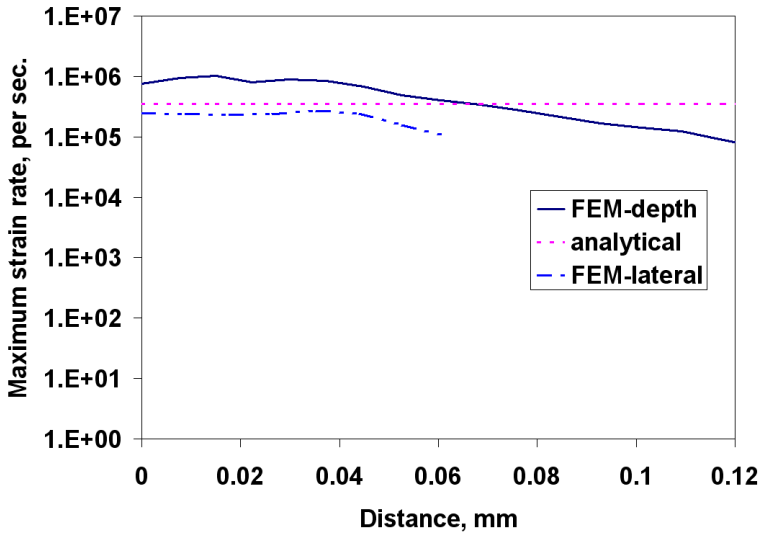


Figure 1: Strain-rate evaluation in shot peening

Then, using the Neuber's approximation (that relates the predicted elastic stresses and strains to the reduced elastic-plastic stresses and strains) and the Johnson-Cook stress-strain relation, the elastic-plastic stresses and strains under loading are calculated. This is reported in 2.1.2. Upon considering the elastic unloading, the final residual stresses due to the single shot are obtained (subsection 2.1.3).

Neuber's equation avoids costly elastic-plastic prediction. It is one of the first and the best approximate models and is used extensively for the last 40 years. It was originally developed for deformation theory. Now, it is used in the incremental form as well and is well researched in the areas of multi-axiality, cyclic loading and creep conditions. The use of Neuber's model avoids the approximation of relating sizes of elastic and plastic indentations to calculate the plastic strain.

Since the velocity of shots does not exceed 100 m/s, the expressions for quasi-static indentation conditions are assumed, but with strain-hardening and rate-dependent stress-strain properties. Strain-rate dependent properties are required as the strain-rate is likely to be  $10^5 - 10^6$  during the peening and most materials show increased dynamic yield strengths due to higher strain rates. Figure.1 depicts the strain-rate evaluated from a single shot impact using FEM along the depth and lateral directions. The strain-rate is plotted till the cold work is present. It varies within the band of  $10^5 - 10^6$ .

Analytically, it is evaluated by the empirical formula  $\dot{\epsilon} = d\epsilon/dt = V/R$  where  $\dot{\epsilon}$  is the strain rate,  $V$  is the shot velocity and  $R$  is the radius (Tuftt, 1997). This result is also marked in the same figure and it is very close the strain rates predicted by FEM. Hence, strain rates evaluated from the empirical formula is used in Johnson-Cook equation for further studies.

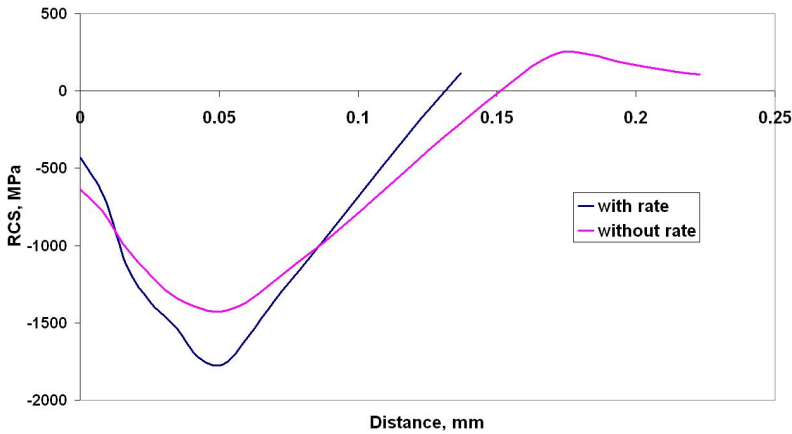


Figure 2: RCS comparison with and without strain-rate properties

Figure.2 shows the RCS from single shot FEM analysis when rate-dependent and rate-independent properties are considered. The RCS is less (and cold work is more) when rate-independent properties are considered. It is clear that consideration of strain-rate properties will provide better results.

In experimental studies conducted by Cammett, Prev y, and Jayaraman (2005), it is reported that the cold work reaches 30% in Inco718 specimens subjected 100% coverage. The intensity reaches 8A (0.2 mmA) level with the CW14 (S110) shots. In a numerical simulation performed by the authors, the cold work reaches high levels. Thus, Johnson-Cook equation, which is valid for generally large plastic strains, is used in the current study.

### 2.1.1 Elastic loading

In order to get the stresses under the loading condition assuming that the material is purely elastic, from Hertz theory, the maximum normal applied pressure,  $p_0$  during loading is given by,

$$p_0 = \frac{1}{\pi} \left[ \frac{5}{2} \pi k \rho V^2 E_0^4 \right]^{1/5} \tag{1}$$

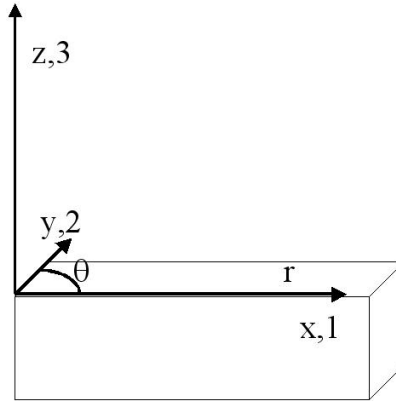


Figure 3: The coordinate systems used in this study

where  $\rho$  is the density of the shot,  $V$  is the initial velocity of the shot and  $k$  is a constant. The maximum radius during the elastic loading,  $a_e$  is given by,

$$a_e = \frac{D}{2} \left[ \frac{5}{2} \pi k \rho \frac{V^2}{E_0} \right]^{1/5} \quad (2)$$

where  $D$  is the diameter of the shot and  $E_0$  is the equivalent elastic modulus of the shot and the target.  $E_0$  is defined by,

$$\frac{1}{E_0} = \frac{1 - \nu^2}{E} + \frac{1 - \nu_s^2}{E_s} \quad (3)$$

where  $E_s$  is the elastic modulus of the shot,  $E$  is the elastic modulus of the target,  $\nu_s$  is the Poisson ratio of the shot and  $\nu$  is the Poisson ratio of the target. The elastic stress field created by the spherical impact is given by,  $\mathbf{T}^e$  (the elastic stress tensor)

$$\mathbf{T}^e = \begin{bmatrix} \sigma_{11}^e & 0 & 0 \\ 0 & \sigma_{22}^e & 0 \\ 0 & 0 & \sigma_{33}^e \end{bmatrix} \quad (4)$$

where  $\sigma$  represents the stress, 1, 2 and 3 represent the three orthogonal coordinate axes, 1 and 2 represent the in-plane coordinates, while 3 represents the impact direction. In a cylindrical coordinate system,  $r$  and  $\theta$  represent the 1-2 plane. The coordinate systems are shown in Figure.3. During loading, the maximum stresses due to Hertzian pressure loads are given by,

$$\sigma_{11}^e = \sigma_{rr}^e = p_0(1 + \nu) \left[ \frac{z}{a_e} \tan^{-1} \left( \frac{a_e}{z} \right) - 1 \right] + p_0 \frac{a_e^2}{2(a_e^2 + z^2)} \quad (5)$$

$$\sigma_{22}^e = \sigma_{\theta\theta}^e = p_0(1 + \nu) \left[ \frac{z}{a_e} \tan^{-1} \left( \frac{a_e}{z} \right) - 1 \right] + p_0 \frac{a_e^2}{2(a_e^2 + z^2)} \tag{6}$$

$$\sigma_{33}^e = \sigma_{zz}^e = -p_0 \left[ 1 + \left( \frac{z}{a_e} \right)^2 \right] \tag{7}$$

In the above equations,  $\sigma_{rr}$ ,  $\sigma_{\theta\theta}$ ,  $\sigma_{zz}$  are the radial, tangential and axial stresses respectively. The shear stresses are negligible along the line of impact and the three stresses can be assumed to be principal stresses. The equivalent Von-Mises stress,  $\sigma_{eq}^e$  is given by,

$$\sigma_{eq}^e = \sqrt{\left[ (\sigma_{rr}^e - \sigma_{\theta\theta}^e)^2 + (\sigma_{\theta\theta}^e - \sigma_{zz}^e)^2 + (\sigma_{zz}^e - \sigma_{rr}^e)^2 \right] / 2} \tag{8}$$

The equivalent strain,  $\epsilon_{eq}$  can be calculated by,

$$\epsilon_{eq}^e = \sigma_{eq}^e / E \tag{9}$$

where  $E$  is the elasticity modulus of the target material.

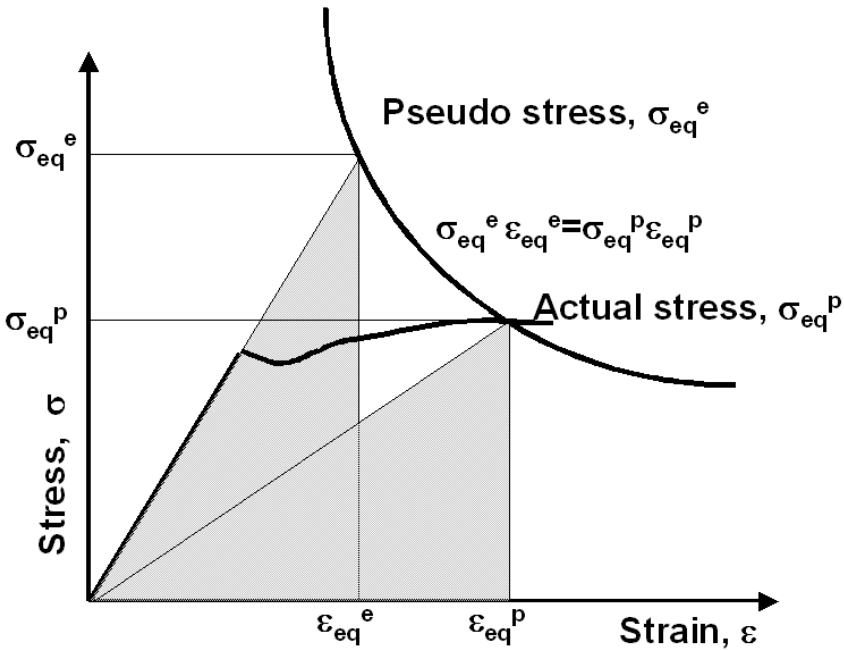


Figure 4: Neuber’s equation that relates pseudo elastic stresses and elastic-plastic stresses. The strain energy due to pseudo-elastic stresses is assumed to be equal to the strain energy due to elastic-plastic stresses.



$$\sigma_{eq}^e \epsilon_{eq}^e = \sigma_{eq}^p \epsilon_{eq}^p \tag{11}$$

In Neuber’s equation, the area under pseudo-elastic stress and strain is matched with the area under actual elastic-plastic stress strain curve. From the two equations, the elastic-plastic stress and strain that produce the same area as the pseudo-elastic stress and strain are determined. The mean stress (or hydrostatic stress) is given by,

$$\sigma_m^e = \frac{1}{3}(\sigma_{11}^e + \sigma_{22}^e + \sigma_{33}^e) \tag{12}$$

The stress deviator  $s_{11}^e$  is calculated as,

$$s_{11}^e = \sigma_{11}^e - \sigma_m^e = \frac{1}{3}\sigma_{eq}^e \tag{13}$$

In the same way,  $s_{22}^e$  is evaluated.  $s_{33}^e$  is evaluated to be  $-(s_{11}^e + s_{22}^e)$  as the first stress invariant,  $J_1 = \Sigma s_{ii}^e = 0$ . Since  $s_{11}^e = s_{22}^e$ ,  $s_{33}^e = -2s_{11}^e$ . The elastic-plastic stress deviators are calculated as,

$$s_{ij}^p = \frac{1}{1+\nu} \frac{\sigma_p}{\epsilon_p} e_{ij}^p = \frac{1}{3}\sigma_{eq}^p \tag{14}$$

As mentioned in the case of the elastic stress deviators, the first stress invariant,  $J_1 = \Sigma s_{ii}^p = 0$  and hence  $s_{33}^p$  is evaluated to be  $-(s_{11}^p + s_{22}^p) = -2s_{11}^p$ .

### 2.1.3 Residual stresses after unloading

The unloading is assumed to be elastic. The residual stress is evaluated as the difference between plastic and elastic stress deviators and given by,

$$\sigma_{ij}^R = \frac{1}{3}(s_{ij}^p - s_{ij}^e) \tag{15}$$

Therefore, the residual stresses,  $\sigma_{rr}^R$ ,  $\sigma_{\theta\theta}^R$ ,  $\sigma_{zz}^R$  are (Figure.5)

$$\sigma_{rr}^R = \sigma_{\theta\theta}^R = \frac{1}{3}(\sigma_{eq}^p - \sigma_{eq}^e) \tag{16}$$

$$\sigma_{zz}^R = -2\sigma_{rr}^R \tag{17}$$

Reverse yielding will be experienced by the target metal if  $\sigma_{eq}^e \geq 2\sigma_{eq}^p$ . The residual stresses considering this reverse yielding is given by (Figure.6),

$$\sigma_{rr}^R = s_{11}^p - s_{11}^e = \frac{1}{3}(\sigma_{eq}^p - 2\sigma_{eq}^p - \Delta\sigma_{eq}^p) \tag{18}$$

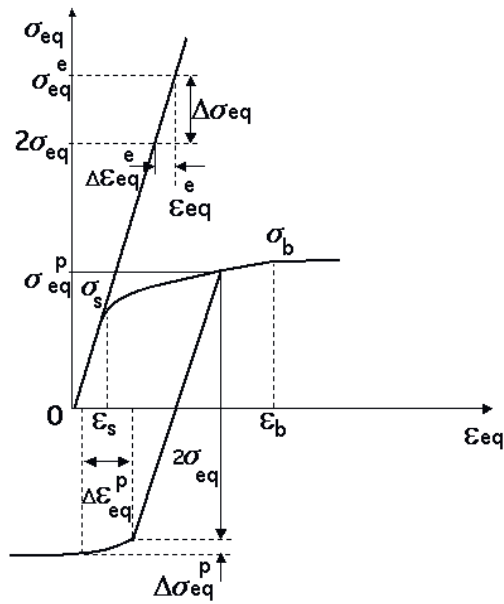


Figure 6: Residual stresses after unloading. The unloading could result in reverse yielding due to Bauschinger effect.

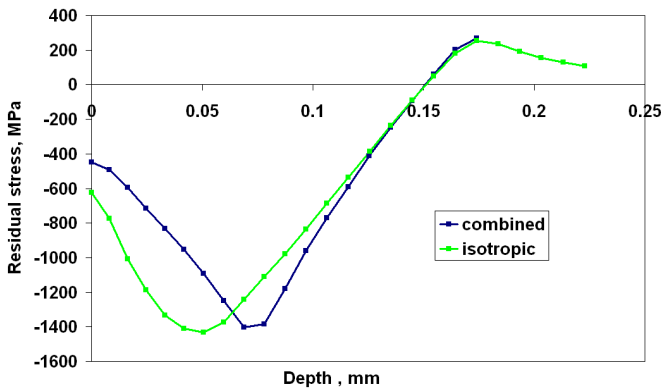


Figure 7: RCS distribution obtained using different material models, These models have used rate-independent stress-strain properties.

$$\sigma_{\theta\theta}^R = \frac{1}{3}(\sigma_{eq}^p - 2\sigma_{eq}^p - \Delta\sigma_{eq}^p) \tag{19}$$

$$\sigma_{zz}^R = -2\sigma_{zz}^p \tag{20}$$

where  $\Delta\sigma_{eq}^p$  is calculated from Neuber's relation and Johnson-Cook equation. Although combined hardening is more appropriate, the isotropic hardening model is used as it is conservative (Figure.7).

### 2.2 Formulation for multiple shots

To calculate these stresses, RCS may be assumed to be uniform and can be averaged over the entire coverage area. Figure.8 shows the residual stresses due to single shot impact by FEM analysis and it can be seen that both surface RCS and maximum RCS vary along the radius of the indentation, and tensile stresses are observed near the edge of the indentation. Hence, when another shot impacts adjacent to this indentation, the RCS must first overcome the tensile stresses. This effect will result in lower average stresses. The plastic strains are averaged along the indentation radius and hence the RCS that is evaluated for 100% coverage is found to be lower than the values for single shot impact.

The in-plane plastic strains are equal ( $\epsilon_{rr}^p = \epsilon_{\theta\theta}^p$ ) as they are assumed to be uniform on the peened surface (Fathallah, Inglebert, and Castex, 1998). Also, incompressibility due to plastic deformation imposes the following condition:

$$\epsilon_{rr}^p + \epsilon_{\theta\theta}^p + \epsilon_{zz}^p = 0 \tag{21}$$

With  $\sigma_{zz}$ ,  $\sigma_{r\theta}$ ,  $\sigma_{rz}$ ,  $\sigma_{\theta z}$  being zero, the residual stresses are functions of only  $z$  coordinate. Thus, the plastic strains are related to the residual stresses by means of:

$$\epsilon_{rr}^p = -\frac{1}{E}(\sigma_{rr}^R(z) - \nu\sigma_{\theta\theta}^R(z)) \tag{22}$$

$$\epsilon_{\theta\theta}^p = -\frac{1}{E}(\sigma_{\theta\theta}^R(z) - \nu\sigma_{rr}^R(z)) \tag{23}$$

The residual stress in  $r\theta$  plane is zero.

$$\frac{1+\nu}{E}(\sigma_{r\theta}^R(z)) = 0 \tag{24}$$

Thus we can relate the residual stresses with the plastic strain,  $\epsilon_{rr}$  as

$$\sigma_{rr}^R = \sigma_{\theta\theta}^R = \frac{E}{1-\nu}\epsilon_{rr}^p \tag{25}$$

The plastic strain distribution along the line of impact is known. In the other locations, it is difficult to express the plastic strain distribution through closed-form

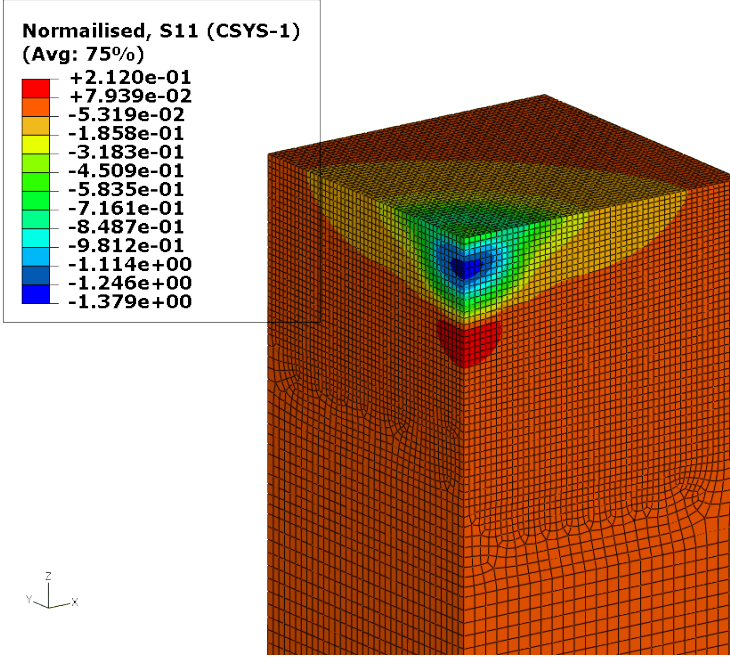


Figure 8: RCS variation due to single impact. Both the surface and maximum RCS values change along the indentation radius and reach a tensile value.

solution. The plastic strain acting at any radius 'r' from the center of impact is assumed to be proportional to the pressure acting at that radius. Based on this assumption, an average plastic strain is evaluated along the radius at a given depth from surface and this is used to evaluate the residual stress distribution at different depths.

$$\varepsilon_{rr}^{p-avg} = \Sigma(\varepsilon_{rr}^p(r))/n \quad (26)$$

where  $\varepsilon_{rr}^{p-avg}$  is the average plastic strain in the indentation and n is the number of summation points.

### 2.3 Probabilistic analysis

Monte-Carlo simulations predict the outcome for the random variations of different input parameters. Stroud, Krishnamurthy, and Smith (2002) have applied Monte-Carlo methods to analyse the effects of parameter random variation in a bonded joint. Renaud and Liao (2007) have calculated the scatter in fatigue lives in different specimens considering the different thicknesses and applied stress character-

istics. In shot peening, parameters such as shot size, velocity, material properties of shot, and target vary in a random manner. The effects of the variations of these parameters on RCS distributions can be determined using the Monte-Carlo method. The random variations of input parameters can be considered to follow a normal distribution. Thus, the designer can verify the extent to which the RCS will vary, given the random variation of the input parameters. The key steps of Monte-carlo method are:

- Build a parametric model connecting peening parameters and the RCS
- Generate a set of random inputs
- Calculate the response for the above set of inputs
- Repeat the last two steps  $n$  times

### 3 Numerical Modeling

The RCS distribution below the surface from analytical model is based on the theoretical contact mechanics and elastic-plastic theories in a semi-infinite medium. The predictions based on the analytical model, viz., the RCS at the surface, the maximum RCS and the depth of maximum RCS need to be verified and validated through FEM analysis. The FEM based unit cell approach has been used by the authors for single and multiple shot impacts. The analytical and the FEM model employ strain-rate dependent elastic-plastic properties. Thus, one can compare the results from analytical and numerical models for identical conditions.

#### 3.1 Materials

In order to validate the analytical results, a unit cell approach is followed with single and multiple shot impacts. The materials used are SAE1070 and Inco718. SAE1070 is a carbon steel used in Almen strip to monitor the peening progress and Inco718 is a well-known superalloy used in aircraft engines. The mechanical properties for these materials are given in Table.1. The rate-dependent properties are given by Johnson-Cook equation, mentioned above. However, in the current study, the effect of increase in temperature due to peening is not included. Therefore, only the constants A,B,C and  $n$  are evaluated for both the materials given in Table.2.

#### 3.2 Finite element modeling

The FEM model is shown in Figure.9. ABAQUS/Explicit software is used for finite element simulation. The target material is modeled as a unit cell whose cross

SI No	Property	SAE1070	Inco718
1	Hardness (HRC)	44 -50	36
2	Yield Strength	1268 MPa (Tufft, 1997)	1036 MPa
3	% Elongation	8.2	12
4	Ultimate Strength	1422 MPa	1240 MPa
5	Density	7800 kg/m <sup>3</sup>	8100 kg/m <sup>3</sup>

Table 1: Properties of SAE1070 steel and Inco718

Material	A	B	C	n
SAE1070	1408	600.8	0.0134	0.234
Inco718	1	5720	10	0.12

Table 2: Material constants of SAE 1070 steel and Inco718

section measures 1 mm × 1 mm. The depth of the cell is equal to 1.25 mm. The cell is modeled with C3D8R (hexagonal elements with reduced integration) elements. The shots are positioned such that they will impact the area at the center of the cell measuring 0.25 mm × 0.25 mm. To capture the stresses properly, very fine meshing is done at the impact area and its surrounding. The entire surface except the top surface is coated with infinite elements to prevent stress waves from propagating back. Material model with isotropic hardening including strain rate is employed.

The shot is modeled as a rigid sphere with 0.1778 mm radius. The shot material is assumed to be made of steel for mass calculations. It is meshed with hexagonal elements, with all elements are connected to its center using a rigid constraint. The shots impact normal to the surface with a velocity of 62.5 m/s. General contact is defined between the top surface of the unit cell and the spherical surfaces of the shots.

### 3.2.1 Single shot simulation

Based on the above details, the FE model is developed. Since infinite elements are used, the residual stress distribution is directly obtained once the shot leaves the top surface. In addition, the diameter of the indentation is also measured for performing multiple shot simulation.

### 3.2.2 Multiple shot simulation

In this simulation, 100% coverage is ensured over an area of 0.25 mm × 0.25 mm. In reality, the shots impact the surface in a random way. A computer program is written to determine the number of shots and their locations to ensure full cover-

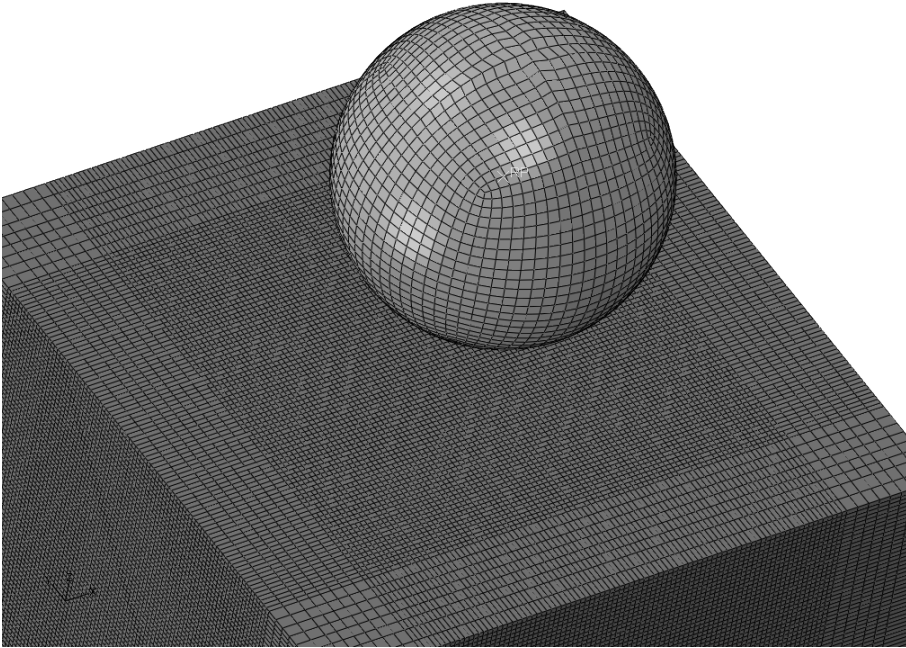


Figure 9: Single shot FE Model

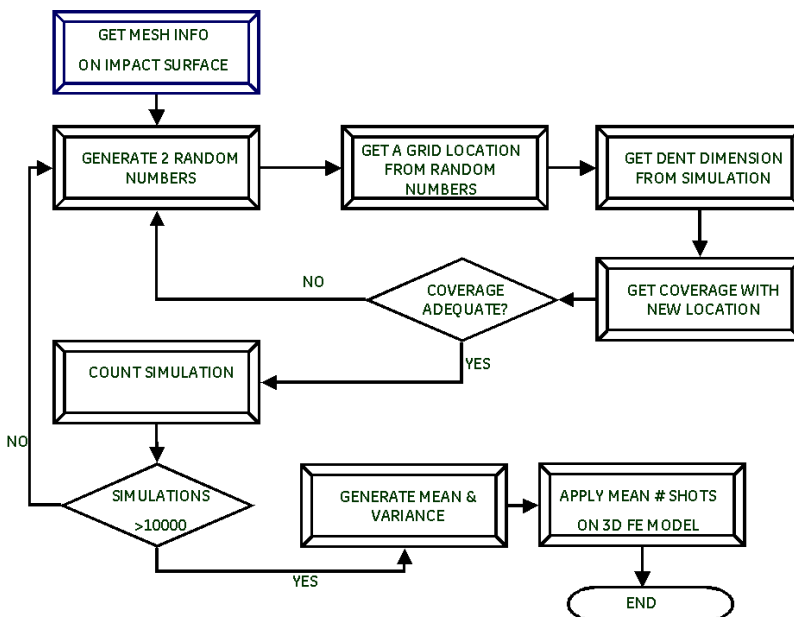


Figure 10: Multiple shot simulation through random process

age. The process is explained in Figure.10. Random numbers are generated using pseudo-random number generation in the XY plane to determine the center of the shots. The number of shots will depend on random number seed. It is likely that sometimes less number of shots will be required for 100% coverage and sometimes more number of shots will be required for 100% coverage. In the case of less number of shots, the simulation time will be less, but less energy is likely to be imparted and vice versa. To get an optimum number of shots, the simulations are repeated 10000 times to determine the mean number of shots and their locations for the coverage. The mesh information in terms of nodal coordinates and element

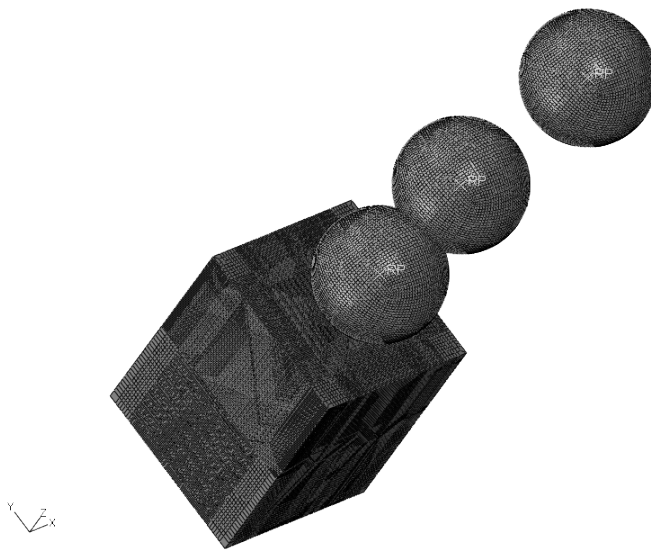


Figure 11: Finite element model with multiple shots. These shots are positioned randomly to have 100% coverage

connectivity are extracted. The node nearest to the impact location is selected and the nodes within indentation radius are blanked out as part of area covered. The process is repeated for each impact and the coverage is calculated and modified. Once the coverage reaches 100% area, the computer program stops. The vertical dimension of the shots is controlled to avoid any interference among them. The number of shots and their spatial locations are used in ABAQUS/Explicit to generate the FEM models for the shots. The FEM mesh with multiple shots is shown in Figure.11. Once all shots impact the surface, the average of residual stresses are

computed at each layer of nodes within the impact zone.

## 4 Results and discussions

### 4.1 Single shot impact

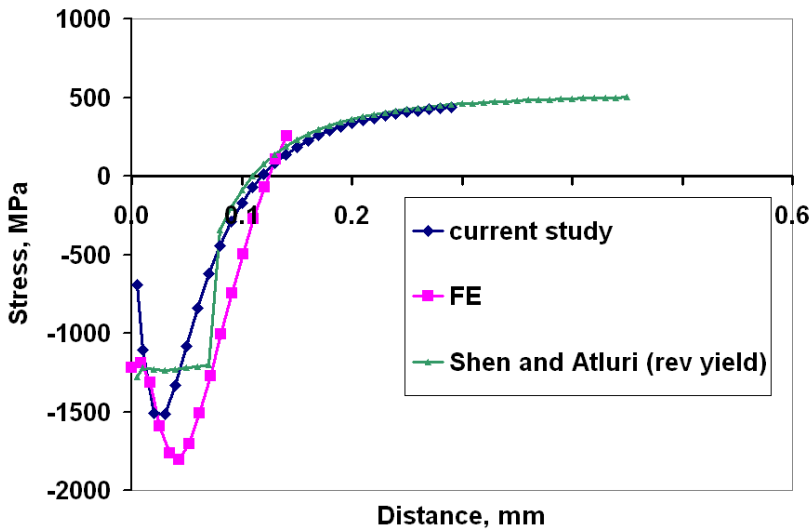


Figure 12: Residual stress prediction in SAE1070 steel due to single shot impact. The impact is normal to the surface. The three curves depict the results from the current study, single impact FEM and Shen and Atluri model considering reverse yielding respectively.

Figure.12 depicts the residual stress distribution in SAE1070 steel due to the single shot impact. The stresses from FEM are compared with the stresses calculated analytically without reverse yielding. The stresses evaluated by analytical method are similar and reasonably close to stresses evaluated by FEM. The curve which represents reverse yielding is truncated once the RCS reaches the yield point. The maximum residual stresses after reverse yielding are very close to the stresses without reverse yielding, but their overall pattern is different from each other. The stresses without reverse yielding match better with stresses evaluated using FEM. Also, the residual stresses turn tensile in the inner material. The FEM predicts deeper RCS in comparison to analytical prediction. The residual stress distributions in Inco718 between FEM and analytical methods are compared in Figure.13 for single shot

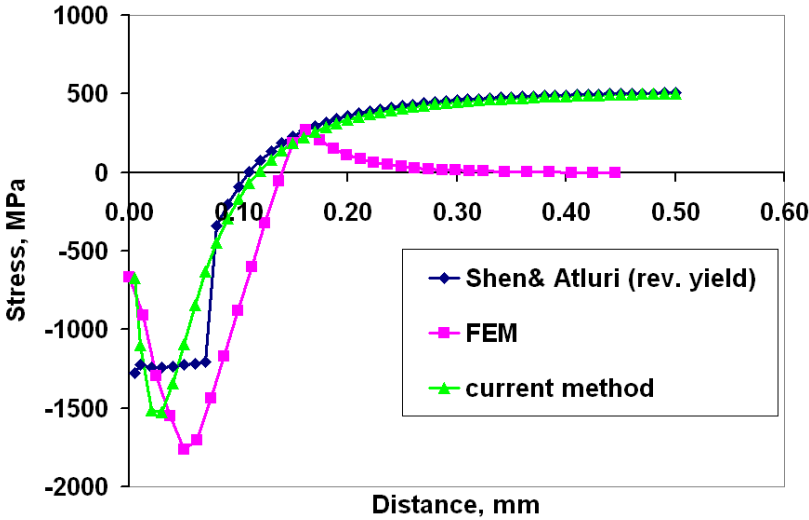


Figure 13: Residual stress prediction in Inco718 due to single shot impact. The impact is normal to the surface.

impact. As in SAE1070 steel, even in Inco718 material, analytical methods predict lower depth for maximum residual stresses.

#### 4.2 Multiple shot impacts

Figure.14 depicts the RCS along the radius of indentation for single shot impact. The stresses from the FEM analysis become tensile at the edge of indentation, indicating that the averaging of stresses due to multiple impacts will be lower than the maximum values. When multiple shots are impacting the surface, the averaged stress distribution is captured in Figure.15. The analytical method which uses average strain (and hence average RCS) approach provides a very close estimate of the residual stresses. The experimental results from (Cammatt, Prev y, and Jayaraman, 2005) are also superimposed on the results. Reverse yielding condition is not reached as the stresses due to multiple impacts are lower than the reverse yielding point. It can be seen that the analytical model predictions are quite comparable with the experimental results. In Figure.16, the RCS variation due to two different shot sizes (0.1778 mm and 0.254 mm radii) are compared. The velocity is kept at 62.5 m/s. As expected, the larger shot size produces deeper and higher RCS than the smaller one.

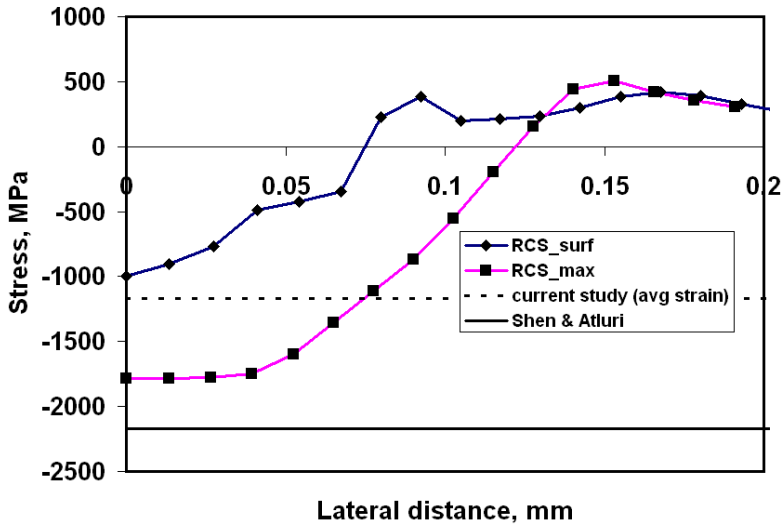


Figure 14: RCS along lateral direction for different configurations. The RCS-surf curve shows the stresses on the surface and the RCS-max shows the maximum stresses from single shot FEM analysis. The other two curves are from the study by Shen and Atluri (2006) and the current study.

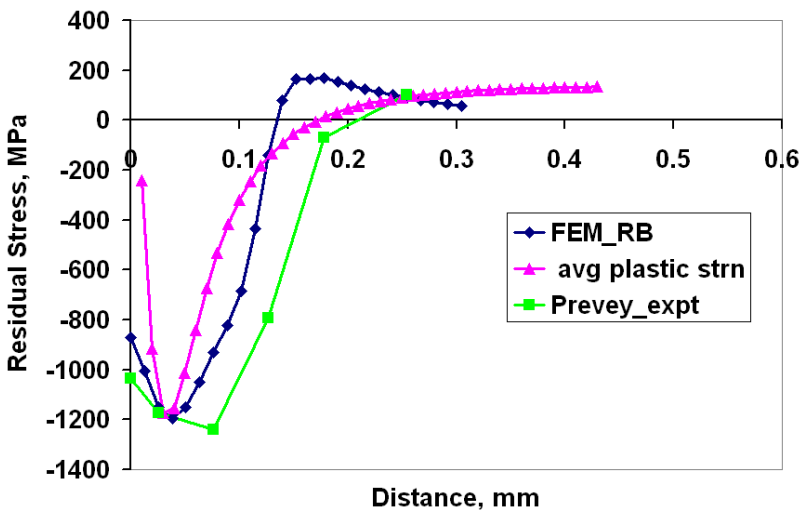


Figure 15: Residual stress prediction in Inco718 due to multiple shots. In the FEM analysis, these shots are positioned randomly to have 100% coverage. The experimental results are obtained from Ref.(Cammett, Prev y, and Jayaraman, 2005).

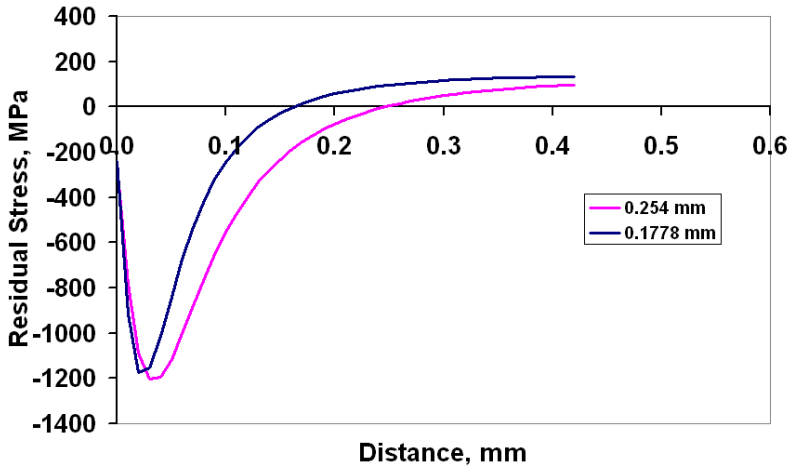


Figure 16: Comparison of RCS due to two different shot sizes. The higher shot size produces more and deeper RCS.

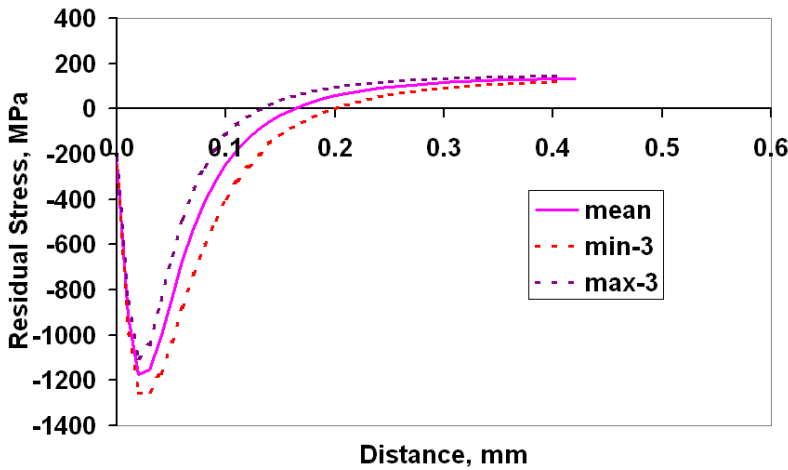


Figure 17: The RCS variation due to shot size and velocity variation in 0.1778 radius. In the Figure., RCS distribution denoted by min3 and max3 represent  $3 \times$  standard deviations.

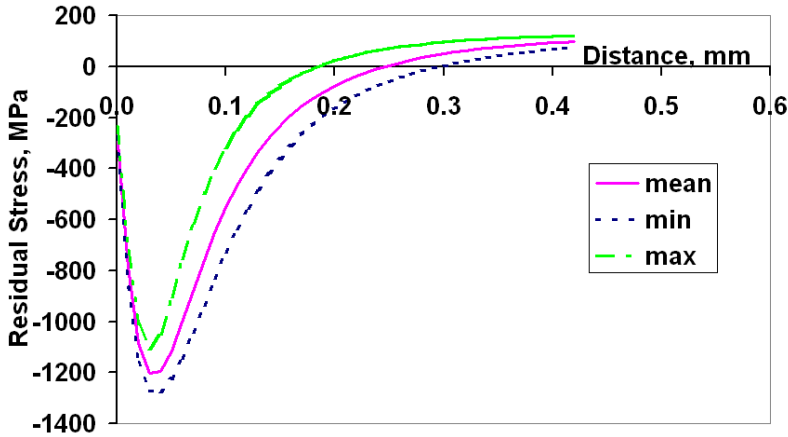


Figure 18: The RCS variation due to shot size and velocity in 0.254 mm radius. The radius is assumed to have a  $3 \times$  standard deviation of 5% of shot radius and velocity, i.e. 0.0127 mm and 3 m/s respectively.

### 4.3 Probabilistic analysis

During operation, all the shots will lose the spherical shape with uniform diameter. Due to the usage, the shots are likely to break into smaller pieces. Sieves are used to ensure the quality of shots, which are being used. For example, for S110 shots, sieve number 35 (aperture of 0.5 mm) must not retain any shots. Sieve number 40 (aperture of 0.425 mm) can retain a maximum of 5% of shots. Sieve number 50 (aperture size 0.3 mm) must retain a minimum of 84% cumulative shots. Sieve number 80 (aperture of 0.18 mm) must not have beyond 6% shots. The effect of such a distribution of shots is difficult to analyse numerically, but analytically the effect can be predicted using Monte-Carlo simulations. The Monte-Carlo simulations have been performed for shot S110 (size 0.1778 mm radius). Figure.17 depicts the variation of RCS due to changes in shot size and velocity. The radius is assumed to have standard deviation,  $3\sigma$  of 0.00889 mm. The velocity is assumed to have standard deviation,  $3\sigma$  of 3m/s respectively. As expected, the RCS is less for smaller shot size and lower velocities. Similarly, the shot size of 0.254 mm radius is simulated with radius and velocity variations. Figure.18 shows the effect of such variations on RCS. The actual measurements of shot sizes during peening operation at different stages can be used to calculate the RCS variation using Monte-Carlo simulations

as mentioned above.

## 5 Conclusions

The current study extends the work done by Shen and Atluri (2006) by including strain-rate effects in the analytical modeling of single shot impact. It also employs the well-known Neuber's relation to calculate the plastic strain. For 100% coverage, it assumes averaging of plastic strain approach to predict the residual stresses. It can be seen that the results compare well with numerical results for two different materials under consideration, viz., SAE1070 and Inco718. The results also correlate well with experimental results for Inco718 material. The method is enhanced to be capable of predicting the random variation of shot size and velocity and it can be further expanded to include more input parameters. Thus, the designer can use this method to predict the RCS quickly to setup the process parameters.

**Acknowledgement:** We like to acknowledge GE Aviation for the support during the project.

## References

- Al-Hassani, S.** (1984): An engineering approach to shot peening mechanics. In *ICSP-2*, pp. 275–282, Chicago.
- Al-Obaid, Y.** (1995): Shot peening mechanics: Experimental and theoretical analysis. *Mechanics of Materials*, vol. 19, pp. 251–260.
- Cammett, J.; Prev y, P.; Jayaraman, N.** (2005): The effect of shot peening coverage on residual stress, cold work and fatigue in a nickel-base superalloy. In *ICSP-9*, pp. 429–435, Paris, France.
- Fathallah, R.; Inglebert, G.; Castex, L.** (1998): Prediction of plastic deformation and residual stresses induced in metallic parts by shot peening. *Materials Science and Technology*, vol. 14, no. 7, pp. 631–639.
- Johnson, K.** (1987): *Contact Mechanics*. Cambridge University Press.
- Li, J.; Mei, Y.; Duo, W.; Renzhi, W.** (1991): Mechanical approach to the residual stress field induced by shot peening. *Materials Science and Engineering*, pp. 167–173.
- Ma, S.; Zhang, X.; Lian, Y.; Zhou, X.** (2009): Simulation of high explosive explosion using adaptive material point method. *CMES: Computer Modeling in Engineering & Sciences*, vol. 39, no. 2, pp. 101–124.
- Niku-Lari, A.** (1981): Shot peening. In *ICSP-1*, pp. 1–21, Paris.

**Renaud, G.; Liao, M.** (2007): Probabilistic modeling of material variability in fatigue crack growth. *CMES: Computer Modeling in Engineering & Sciences*, vol. 1, no. 2, pp. 87–92.

**Shen, S.; Atluri, S. N.** (2006): An analytical model for shot peening induced residual stresses. *CMC: Computers, Materials and Continua*, vol. 4, no. 2, pp. 75–85.

**Stroud, W. J.; Krishnamurthy, T.; Smith, S. A.** (2002): Probabilistic and possibilistic analyses of the strength of a bonded joint. *CMES: Computer Modeling in Engineering & Sciences*, vol. 3, no. 6, pp. 755–772.

**Tufft, M.** (1997): *Development of a Fracture Mechanics/Threshold Behavior Model to assess the Effects of Competing mechanisms induced by Shot Peening on the Cyclic Life of a Nickel Based Superalloy, Rene-88DT*. Ph.D thesis, University of Dayton, 1997.